Title

Comparison of frustum confining vessel (FCV) and full-scale testing for helical and expanded piles geotechnical performance

Authors

Esmailzade, Mohammad

Eslami, Abolfazl

McCartney, John S

Publication Date

2024-04-08

DOI

10.1080/1064119x.2024.2330003

Peer reviewed

Comparison of Frustum Confining Vessel (FCV) and Full-Scale Testing for Helical and Expanded Piles Geotechnical Performance

M. Esmailzade[1], A. Eslami[2] & J. S. McCartney[3]**

1- Ph.D. Candidate, Dept. of Civil and Environmental Eng., Amirkabir Univ. of Tech., Tehran, Iran.
E-mail: Es.mo167@aut.ac.ir

2- Professor, Dept. of Civil and Environmental Eng., Amirkabir Univ. of Tech., Tehran, Iran
& Visiting Scholar, Univ. of California San Diego, USA (Abeslami@ucsd.edu).

3- Professor, Dept. of Structural Eng., Univ. of California San Diego, USA. E-mail: mccartney@ucsd.edu

Corresponding author: E-mail: afeslami@aut.ac.ir

Abstract: This study focuses on investigating the compression and pullout load-displacement characteristics of various pile types using a frustum confining vessel at Amirkabir University of Technology (FCV-AUT) and full-scale tests. The FCV-AUT provides a versatile platform for physically modeling reduced-scale deep foundations in a laboratory setting, accounting for flexible geometric and stress factors, and the full-scale load tests took place at two research sites situated along the southern coastline of the Caspian Sea. A comprehensive dataset comprising 40 model-scale and 15 full-scale load tests on different pile configurations (including conventional, helical, and expanded piles) installed in sands has been compiled to facilitate a geotechnical performance evaluation. Conventional piles, encompassing cast-in-place drilled shafts, H piles, pipe piles, and box piles, were considered in the analysis. Helical piles with one to three helixes and various expanded piles, including self-expanded, bubble, and wing piles, were also examined. Notably, among the tested piles, those installed through jacking and expanded piles displayed the highest resistance to compression. Conversely, helical piles and expanded piles demonstrated superior pullout performance when compared to conventional piles. Comparisons between physical model-

scale tests and full-scale tests validate the suitability of FCV-AUT for assessing the geotechnical performance of diverse pile types in sand under realistic stress conditions.

Keywords: Frustum Confining Vessel (FCV), Helical and Expanded Piles, Sand, Load-Displacement records, Scale up

Symbol	**Description**
q_c	Cone resistance for CPT
f_s	Sleeve friction for CPT
σ_v	Vertical stress
σ_h	Horizontal stress
SP	Poorly graded sand
D_{50}	Diameter for 50% finer by weight
e_{max}	Maximum void ratio
e_{min}	Minimum void ratio
$\gamma_{d,max}$	Maximum dry density
$\gamma_{d,min}$	Minimum dry density
G_s	Specific gravity
c_u	Coefficient of uniformity
c_c	Coefficient of curvature
ω_{opt}	Optimum water content
D_f	Embedded depth
L	Pile length
d_s	Pile shaft diameter
d_h	Helix diameter
S	Space between two helices
S/D	Space ratio
L_m	Length of the model pile
L_p	Length of the prototype pile
λ_L	Dimension scale factor

λ_A	Area scale factor
λ_V	Volume scale factor
λ_M	Mass scale factor
λ_ρ	Density scale factor
λ_σ	Stress scale factor
λ_ε	Strain scale factor
λ_F	Force scale factor
λ_E	Modulus scale factor

1. Introduction

The use of deep piles in civil engineering projects has indeed seen a significant increase in recent years, primarily due to the presence of problematic soils and the need to address challenging environmental conditions (Fellenius 2004; Byrne and Houlsby 2015). Various factors play a role in classifying deep piles, including pile material, geometries, load transfer, embedment depth, soil displacement during installation, environmental conditions at the site, installation angle, and the installation method (Ebrahimipour and Eslami 2024). Of these factors, the installation method stands out as a highly influential factor that can profoundly impact pile behavior (Eslami et al. 2020). It affects the behavior of the surrounding soil, the interaction between the soil and the pile (pile-soil interaction), and even the structural behavior of the pile (Paik and Salgado 2004; Basu et al. 2014; Basu et al. 2010). In geotechnical practice, a wide range of pile installation methods are available, each with its own advantages, disadvantages, and suitability for specific project conditions. These methods include driving, drilling, jacking, vibrating, screwing, jetting, suction, grouting, drilling, displacing, and combined methods.

By considering various installation methods, piles can be categorized into two main groups: conventional and unconventional piles (Fattah and Al-Soudani 2016). Conventional piles encompass those that have been traditionally executed using well-established methods, resulting in more familiar behaviors. These methods typically include driving, drilling, jacking, and vibrating. On the other hand, unconventional piles comprise post-grouted, expanded, drilling displacement, jetting, and helical piles, which involve innovative approaches to pile installation (Fattah, Zbar, and Mustafa 2017). The utilization of unconventional piles has garnered significant attention from researchers and engineers as a means to address the limitations associated with conventional piles. However, it's important to note that unconventional piles introduce greater uncertainties and complexities when it comes to predicting their geotechnical performance. Nonetheless, they have the potential to exhibit superior stiffness or ultimate resistance, primarily due to their unique geometry or innovative installation methods. This enhanced performance can lead to substantial cost savings, reduced project duration, and mitigation of environmental and operational challenges, particularly in large-scale projects.

Helical piles, which utilize their distinctive installation approach, demonstrate excellent pullout performance. Consequently, they have gained widespread adoption and are extensively employed in offshore projects. (Byrne and Houlsby 2015; Spagnoli et al. 2015; Gavin, Doherty, and Tolooiyan 2014; Spagnoli 2013). Helical piles exhibit a reduced capacity compared to displacement piles. However, they come with several advantages, including cost-effectiveness, rapid installation, minimal noise and vibration generation, compatibility with commonly available equipment, reusability, and ease of integration in urban environments. (Spagnoli and Gavin 2015; Kurian and Shah 2009; Perlow 2011). Two distinct failure modes have been identified in the case of helical piles, depending on their helix spacing to diameter ratio (S/D) (Lanyi-Bennett and Deng

2019; Livneh and El Naggar 2008). When this ratio surpasses 3, the failure mode is categorized as individual, wherein each helix functions independently, and the total bearing capacity is the cumulative result of each helix's individual bearing capacity. Conversely, for ratios less than 3, the failure mode is described as cylindrical, where a cylinder with a diameter equivalent to the average helix diameter is taken into consideration. (Tang and Phoon 2016; Fateh et al. 2018; Arabameri and Eslami 2021).

The primary concern with helical piles lies in the soil disturbance that occurs during installation, resulting in a significant reduction in pile resistance, as noted by (Lutenegger and Tsuha 2015). To address this issue, several solutions have been proposed, including the post-grouting process, the incorporation of a conical central shaft, and the use of helices with varying diameters, as discussed by (Mansour and El Naggar 2022; Nabizadeh and Choobbasti 2017; Khazaei and Eslami 2017). Another effective solution for mitigating soil disturbance is the implementation of expanded piles. In these piles, the helix or expansive segment is integrated into the pile body or central shaft and expands after installation to reach the desired depth. This approach, unlike traditional helical piles, minimizes soil disturbance in the upper part of the expansive segment, thereby enhancing pile performance, particularly under tensile loads (pullout capacity). The installation of expanded piles can be conducted through various methods, including vibration, screwing, jacking, driving, or a combination thereof. It's worth noting that an increase in both the embedment depth and the diameter of the expansive segment contributes to higher bearing capacity, as observed by (Shojaei et al. 2021; Fattah et al. 2020; Al-Suhaily et al. 2018).

In addition to weighing the pros and cons of various methods, evaluating and comparing different methodologies can be an expensive and impractical endeavor, especially when instrumentation is required. As a result, researchers tend to opt for the examination of the responses of these geotechnical structures using scaled-down models, such as 1g or centrifuge physical models, which permits parametric evaluations to be performed (Fakharian et al. 2022; Fattah et al. 2020; Hajitaheriha et al. 2021). Physical modeling spans a range of scales and research domains, encompassing investigations from model-scale piles to full-scale assessments, to calibrate behavior under realistic conditions, as highlighted by (Liu et al. 2020). In the laboratory setting, various apparatuses are employed to study the performance of foundations, especially piles (Eslami et al. 2023). These include simple chambers (1g), calibration chambers (CCs), centrifuge apparatus (ng), and frustum confining vessels (FCVs) (Esmailzade et al. 2022; Khazaei and Eslami 2016; Karimi et al. 2017).

FCVs typically have a conical or frustum-shaped chamber with an open top and a closed bottom, which was first designed and fabricated at McMaster University (Horvath and Stolle 1996; Sedran 1999; Bak et al. 2021). In 1999, the second apparatus of this kind was constructed at the University of South Florida [Mullins et al., 2001]. The largest FCV, recognized as FCV-AUT was constructed at Amirkabir University of Technology, in 2012 (Shirani et al. 2023). The dimensions of FCV-AUT are larger in comparison with the previous FCVs at McMaster and USF, facilitating investigations of larger piles, leading to a reduction in the errors and limitations relevant to scale effects and boundary conditions [Fateh et al., 2017; Karimi et al., 2017; Khazaei and Eslami, 2016a; Zare and Eslami, 2014].

This study involves an evaluation of the load-displacement curves of different types of piles subjected to both compression and pullout loading. The primary focus is on helical piles, drawing comparisons with conventional and expanded piles. Additionally, two distinct methods for scaling up the load-displacement curves derived from FCV tests on helical piles are scrutinized: one considering stress similarity (as proposed by Sedran in 2001) and the other examining stress discrepancy (as explored in this study). The findings underscore the efficacy of employing FCV results not only for comparative analyses among different pile types but also for predicting actual load-displacement curves in field tests.

2. FCV Testing Concept and Scaling Theory

The Frustum Confining Vessel serves as a hybrid of a calibration chamber and a centrifuge apparatus, making it a versatile tool for conducting physical modeling of deep foundations within a laboratory setting. This device adopts a truncated cone shape and exerts a consistent pressure at its base, resulting in a linear distribution of stress along its central vertical axis. This unique feature distinguishes FCVs as valuable tools, effectively mimicking real-world field conditions, including overburden and lateral stress. In this configuration, the soil is displaced upward through the use of a flexible membrane, developing reactive stresses against the lateral walls. As a result, the vertical stress at the soil's surface remains at zero, gradually increasing with depth until it aligns with the applied pressure at the vessel's base via the pressure system.

Therefore, the FCV device offers certain advantages over 1g laboratoryand centrifuge modeling when it comes to simulating geotechnical and structural behavior. The frustum shape of the vessel allows for more accurate replication of the lateral stress conditions in the ground during pile installation, which can be challenging to achieve in 1g models. In addition, FCV experiments are generally more cost-effective than centrifuge experiments. Constructing and operating a centrifuge facility can be expensive and logistically challenging. FCV setups are typically more accessible and affordable.

While the Frustum Confining Vessel effectively replicates linear variations in stress components with depth, it is essential to scale up the findings obtained from the FCV to deduce the pile-soil response at the full-scale level. Bridging the gap between a model and its prototype using dimensionless parameters is a standard practice in both engineering and science. This practice ensures that the behavior observed in a scaled-down prototype faithfully represents the behavior of the corresponding full-scale model. This procedure is commonly referred to as "similitude" or "similarity analysis" which is introduced by Buckingham's 'Pi' theorem (Buckingham 1914). The fundamental concept involves employing dimensionless parameters that encompass the pertinent physical properties and scales in both the model and the prototype, enabling a meaningful correlation of their behaviors.

The deformational response of sandy soils in the context of the soil-pile interface under various loading conditions can be influenced by several factors (Garnier et al. 2007; Kumar 2007). These factors encompass relative density, the confining effective stress, stress history, the fabric and morphological characteristics of the soil, and the roughness of the pile surface. Consequently, Sedran et al (2001) proposed the adoption of consistent relative density (or the same mass density) and stress conditions between the FCV model and the prototype (i.e., the real-world field conditions). To achieve this consistency and ensure constitutive similarity, the scaling factors for mass density and stress conditions, denoted as λ_ρ and λ_σ respectively, are both set to 1, aligning with the principles (so-called constitutive similarity) articulated by (Baker et al. in 1973). Therefore, the length of the reduced-scale pile can accordingly be derived through

$$L_p = L_m \lambda_L \qquad [1]$$

where L_m and L_p are the lengths of the pile in the FCV model and prototype, respectively; λ_L is the dimension scale factor. The other scaling factors for FCV testing conditions were suggested by Sedran et al (2001) as outlined in Table 1. As can be seen, the other factors are defined as a function of λ_L.

To achieve constitutive similarity, the FCV results must align with field data in terms of mass density and stress state. This means that each FCV result can be seen as a representation of an individual pile in the field, which presents a practical limitation. Nevertheless, real-world engineering needs often go beyond this and require a deeper insight into bearing capacity and load-displacement curves across a broad range of field conditions, including variations in pile length or diameter. To address this limitation, a new set of scaling factors becomes necessary. Although these factors may not strictly adhere to constitutive similarity, they can yield reasonable results as long as the difference in stress conditions between the FCV and the intended field data isn't too significant, thereby avoiding a fundamental mismatch in deformation behavior.

The suggested method maintains the same methodology previously discussed but with a limited discrepancy between the stress state ($\lambda_\sigma \neq 1$). As the stress-dependency of sandy soils is complex, therefore, it is possible to propose a strict limitation for λ_σ to fairly satisfy the constitutive similarity.

Given this assumption, the scale factors can be expressed accordingly which are outlined in Table 1. The details of the derivation used for each scale factor are elaborated in the appendix for further clarification. The scale factors corresponding to the displacement, dimension, area, volume, mass, strain, and density are equivalent to those derived by Sedran et al (2001). The scale factors for the other parameters can be expressed as follows:

The scale factor for stress is treated as λ_σ which is not necessarily equal to 1. The force scale factor (i.e., λ_F) can be expressed as follows:

$$\lambda_F = \lambda_\sigma \lambda_L^2 \quad [2]$$

The modulus scale factor can be expressed as follows:

$$\lambda_E = \lambda_\sigma \quad [3]$$

3. Testing Device and Methodology

3.1 Testing Device (FCV-AUT)

The FCV-AUT apparatus, designed by Zare et al. (2014), stands at a height of 1 meter and features a central division to simplify sample preparation (see Fig. 1). This device exhibits a varying diameter, starting at 300mm at the top and expanding to 1300mm at the bottom. The lower bladder consists of a rubber membrane and is pressurized using an air compressor capable of generating up to 10 bar of pressure. The proposed pressure is regulated and then transmitted to the water-air tank via a regulator. The bladder, characterized by its elastic behavior, expands under the applied pressure and transfers this force to the soil (Fig. 2).

Notably, the bladder within the FCV-AUT setup can accommodate vertical stresses of up to 300 kPa. This stress level corresponds to an overburden equivalent to approximately 15 meters of soil with a unit weight of 20 kN/m^3.

The horizontal stress is one of the most critical parameters in determining the friction capacity of piles. It is essential to consider it as a significant factor in determining the behavior of the pile in physical modeling and Experimental studies. Jardine et al. 2013 used a calibration chamber to simulate the stress condition within a large soil element hosting the pile installation (Jardine et al. 2013). It should be noted that due to the conical shape of the FCV device, stress distribution within it varies linearly with depth, in both the vertical and horizontal directions. When pressure is applied to the bottom of the FCV device, the stress reactions induced by its body exhibit almost linear variations not only vertically but also horizontally with depth.

To assess the stress distribution within the FCV chamber, four sensors were employed, positioned in two orientations: vertical and horizontal. These sensors were tasked with measuring both vertical and horizontal stresses in the soil, respectively. The measurement of stress at different elevations (specifically, at 200, 400, 600, and 800 mm from the bottom) was accomplished using digital pressure meters. This enabled the determination of stress distribution within the soil under conditions consistent with the intended field stress condition, as shown in Fig. 3. The outcomes, as depicted in Fig. 4, reveal that horizontal and vertical stresses exhibit linear variations with depth as required. To conduct a more comprehensive assessment of the sampling process and the performance of the FCV-AUT device at various depths, a series of cone penetration tests (CPTs) were carried out for two distinct initial density conditions. As depicted in Fig. 5, as the depth increased, along with the corresponding rise in effective overburden and relative density, both tip and shaft resistance (q_c & f_s) exhibited an upward trend, highlighting realistic simulation of both stress and void ratio distributions.

3.2 Tested Materials

Numerous FCV tests were conducted on various types of piles, employing two sandy soils obtained from the coastal areas of Anzali and Babolsar beaches along the southern shores of the Caspian Sea. The first location, Bandar Anzali, is situated near a prominent commercial port in Iran, with geographical coordinates of 37.4639 N and 49.4799 E, approximately 10 meters below the free water level. The shoreline extends as a narrow strip for about 40 kilometers, primarily composed of fine sand matching the region's soil characteristics. Anzali sand falls into the category of poorly graded sand according to the Unified Soil Classification System (USCS), and its corresponding grading curve is displayed in Fig. 6(a). Fig. 6(b) presents a scanning electron microscope (SEM) image of Anzali sand, while Table 3 summarizes the key properties obtained from laboratory tests for Anzali sand.

The second material was sourced from Babolsar city, situated at coordinates 36.7005° N and 52.6502° E, known for its distinctive sandy soil in Iran. Babolsar serves as both a prominent commercial port and a popular tourist destination, which explains the prevalence of heavy construction activities there (Kaviani-Hamedani et al. 2024). The soil in Babolsar is categorized as poorly graded sand (SP) according to the USCS, and its corresponding grain size distribution curve is depicted in Fig. 6(c). A close-up grain-scale snapshot of Babolsar sand is provided in Fig. 6(d). The major relevant properties of Babolsar sand are summarized in Table 2. It should be pointed out that some field tests were also carried out on both sites which are briefly described in the following sections.

3.3 Sample Preparation

Sample preparation was conducted using the wet tamping technique, maintaining the sand's gravimetric water content at a constant 4%. To achieve the desired initial relative densities, precise portions of soil were methodically layered in 50 mm increments and gently placed into the FCV. Each layer underwent compaction using a wooden rammer until the target density was reached. To ensure the uniformity of the sample, measuring tapes are installed on four sides on the inner wall of the FCV chamber to prevent excessive tamping and ensure that the density remains consistent with the desired level. Additionally, the soil height in the central parts of the device is continuously monitored during sampling from the top of the chamber.

This layering and compaction procedure continued until the soil elevation reached 100 mm, as depicted in Fig. 7. Subsequently, soil placement and compaction persisted until the soil height reached the final 1000 mm height. At this stage, the proposed pressure was adjusted using the regulator, and the valve for fluid transfer to the bottom of the FCV was opened, subjecting the soil to pressure. It's worth noting that a 30-minute time interval was adhered to ensure the even distribution of pressure throughout the soil.

Another method used to verify soil density involves the use of a small sampler. A tube with a diameter of 43 mm and a length of 100 mm is selected for this purpose. As can be seen, a thin-walled, sharp-tipped tube is derived into the soil to take a sample in an undisturbed manner. Consequently, the relative density of the layers is determined by Weight-Volume relationships. This procedure was conducted at different locations to ensure that the intended relative density was achieved in a homogenous manner across the chamber.

3.4 Piles Installation Methods in FCV

Various pile installation methods were employed in this study. To install precast-in-place piles, a 90 mm diameter hole was first bored at the center of the FCV chamber using a casing. The pile was then carefully positioned vertically within the hole. Subsequently, the space between the pile and the hole walls was filled with highly fluid concrete, as depicted in Fig. 8(a). In the case of bored piles, a 90 mm diameter hole was also drilled, and then it was filled with concrete. To facilitate tensile testing, a 16 mm diameter steel bar was centrally embedded within the pile, as shown in Fig. 8(b).

The category of driven piles are comprised of four distinct pile shapes: open-end pipe, closed-end pipe, H-shaped, and steel box. These piles were initially positioned at the soil surface. After ensuring their vertical alignment, they were then driven to a depth of 750 mm using a steel hammer. On the other hand, jacking piles were installed with the assistance of a hydraulic jack, providing a course of 1000 mm and a capacity of 10 tons. To guarantee the verticality of these piles, a wooden fixer was employed. Additionally, a level was used to maintain the alignment of the pile, as illustrated in Fig. 8(e).

As for helical and expanded piles, the installation process involves the application of a torque motor to the pile head concurrent with the assignment of axial loads. This operational method was conducted by utilizing a torque motor, as visually represented in Fig. 8(e). The axial load was assigned via two pneumatic jacks situated on the sides of the pile, while a rotating motor connected to the pile head was responsible for generating the required torque moment. The precise measurement of the torque required for pile installation is meticulously conducted through a torque meter integrated with the pile head. Furthermore, this apparatus is equipped with a depth meter sensor that diligently records the penetration rate and velocity at a consistent interval of two seconds. Throughout the pile installation procedures, all depth meter and torque meter sensors are intricately linked to a data logger, thus facilitating the systematic recording of the installation torque versus depth diagram.

"The bearing capacity and pile behavior are significantly influenced by the pile installation method as reported by Baca & Brzakala (2017) and Heins et al. (2020). In real-world engineering, piles are generally installed into an existing field in which the stress along different directions is distributed (Heins et al. 2020; Baca and Brzakala 2017). In the FCV device, the bottom pressure is generally applied before pile installation, simulating the prototype stress condition. Otherwise, it would be the wrong representative. Moreover, to ensure uniform pressure distribution across the entire sample, there has been a minimum 30-minute interval between sample preparation and pile installation. It should be noted that the embedment depth of all piles 750 mm was adopted regardless of pile type.

3.5 Loading Procedures

The pile loading was conducted using the rapid loading method as per ASTM D1143 and ASTM D3689 standards. In this approach, the ultimate pile capacity is initially estimated and then divided into twenty equal segments, with 5% of the ultimate capacity applied to the pile in each loading increment. During each stage, the pile is held for 10 minutes while simultaneously recording any settlement of the pile. To impart axial compression and tension loads (representing the pullout loading path), a reciprocating hydraulic handy jack with a capacity of 150 kN and a 150 mm course was utilized. The load applied to the pile head is quantified using an S-shaped load cell capable of measuring up to 100 kN. Furthermore, an LVDT (Linear Variable Differential Transformer) with a 100 mm course and an accuracy of 0.01 mm was employed to monitor the displacement of the pile head. All data acquired from the load cell and LVDT is meticulously collected and recorded by a sixteen-channel datalogger. This data logger is configured to store force and displacement values at five-second intervals. Fig. 9 illustrates the connection of the LVDT and load cell to the piles.

4. Introducing FCV-AUT Database

Over the span of a decade from 2013 to 2023, a series of experiments were carried out at the FCV-AUT facility to investigate the behavior and performance of various types of piles under both compressive and tensile loads. The piles examined encompassed closed-end and open-end pipe piles, conventional H-shaped piles, helical piles with 1 to 3 helices, and self-expanded special piles. These model piles were carefully installed in two distinct sand samples collected from the Anzali and Babolsar sites, representing a wide spectrum of relative densities. The experiments covered a range of essential parameters, including embedment depth, helix diameter, the ratio of helix spacing to diameter, the impact of installation methods, soil disturbance extent, and potential solutions to encountered challenges. The culmination of these research endeavors is a comprehensive database named the FCV-AUT database, which is introduced and expounded upon in this study. For more precise details regarding pile characteristics, deposit properties, and types of loading, please consult Table 3.

5. Load-Displacement Records

5.1 Conventional Piles

Repeatability assurance of conducted tests is one of the most important and notable issues in physical modeling. In this regard, three distinct compressive and pull-out loading tests on Helical piles were conducted with FCV-AUT apparatus to ensure the repeatability and reliability of the results. The load-displacement data from the different tests are shown in Fig. 10. The results for both compression and pull-out loading paths are practically consistent in terms of load-displacement results, highlighting the high repeatability and reliability of apparatus in the physical modeling of piles.

Fig. 11(a) shows the results of load-displacement curves for FCV compressional tests with conventional piles, including jacked and driven closed-end, open-end, and an H-shaped pile accompanied by driven concrete and box-shaped piles.

As exemplified in Fig. 11(a), a conspicuous disparity emerges, wherein the ultimate compressive load capacity of piles installed via the jacking method markedly exceeds that of piles installed using the driving method. This marked difference can be primarily attributed to the substantial soil disturbance incurred during the driving process for piles. Notably, when considering a bearing capacity index equating to 10% of the pile diameter, it becomes apparent that piles installed through the jacking method exhibit an approximately twofold increase in their bearing capacity compared to their driven counterparts. In the context of initial stiffness, a similar discrepancy in performance is observed between jacked and driven piles, except for open-end piles. It is of significance to note that, intriguingly, the load-bearing capacity of driven concrete piles surpasses that of steel piles. This apparent incongruity can potentially be ascribed to the surface roughness of concrete piles, which contrasts with the relatively smoother surface of steel piles.

In this research, one of the variables under investigation involves analyzing the impact of installation methods on pile behavior, encompassing various techniques. Among these methods, the precast-in-place pile method has been examined. As you noted, during the execution of these piles, stresses within the soil are relieved from drilling to pile installation, leading to a loss of pile skin friction. Consequently, this method is relatively uncommon, and the findings suggest that it typically yields low capacities.

Similarly, Fig. 11(b) illuminates the same load-displacement curves but under pull-out loading. The results indicate that the distinct difference between the loading bearing capacity of jacked and driven piles observed under compression loading is depreciated under tensile loading. Overall, it can be observed that the bearing capacity and initial stiffness of conventional piles are a function of the installation method for each pile shape.

5.2 Helical Piles

In Fig. 12(a) and 12(b), load-displacement curves for helical piles in loose and medium-density sandy soils are depicted. These piles differ in terms of the number (1, 2, 3), diameter (64, 70, 90 mm), and space ratio (S/D=1.5 and 3) of the helices installed on the pile surface. Each test is clearly labeled, indicating the number of helices, helix diameter, space ratio, and the type of tested soil. For instance, the test name "2H, 90, S/D=3, Anzali" denotes a pile with two helices having a diameter of 90 mm and a space ratio of 3, which was tested in Anzali sand.

Tsuha (2013) revealed that the space ratio plays a crucial role in altering the failure pattern in helical piles as the S/D ratio increases. As the S/D ratio reaches 3, helical piles are anticipated to function individually, while at S/D=1.5, cylindrical failure is more likely to occur (Tsuha et al. 2013).

The results presented in Fig. 12 illustrate that among the tested configurations, the pile is characterized by three helices, each with a diameter of 90 mm and a space ratio of S/D=3, exhibiting the highest bearing capacity. This particular configuration is expected to function as an individual unit, with its bearing capacity surpassing that of a single helical pile.

Conversely, the lowest bearing capacity is observed in the case of a single helical pile. Notably, as the number of helices increases, the enhancement in bearing capacity becomes less pronounced. Specifically, there is a diminishing difference in bearing capacity between configurations with two helices (2H) and those with three helices (3H), provided they share the same space ratio. This observed trend can be attributed to the substantial influence of the deepest helix on bearing capacity in comparison to the second and third helices, which are positioned at higher elevations where lower stress levels are expected. Moreover, the deepest helix operates with minimal soil disturbance compared to the others. Both the 2H and 3H configurations have their helices positioned at the maximum and intermediate embedded depths. Therefore, the addition of an extra helix in the 3H configuration, situated at a higher elevation (i.e., the shallowest embedded depth), does not yield a significant difference in terms of bearing capacity. During the installation of helical piles, the rotational movement of the helices causes significant disturbance to the soil. With each helix penetrating the soil, this disturbance intensifies. Consequently, the soil at higher elevations experiences a greater number of helic passages. For example, in a three-helix pile, the soil beneath the lower helix remains relatively undisturbed as it is not directly affected by the helix.

However, beneath the middle-level helix, the soil has already been disturbed by the passage of the lower helix. Similarly, the soil beneath the higher-level helix undergoes disturbance twice: once by the lower-level helix and once by the middle-level helix. Therefore, the majority of the load is transferred by the lowest helix. Similarly, the results of helical piles under pullout loading tested on loose and medium-density soils are presented in Figs. 12(c) and 12(d), respectively.

Under pullout loading, the number of helices and space ratio play a significant role in the load-displacement curve. As can be seen for helical piles with the same helix diameter and number of helices, the bearing capacity and initial stiffness decrease with the space ratio, signifying the systematic altering in failure mode from individual to cylindrical.

Fig. 13, the upward movement of a helix under pullout loading tends to develop a passive wedge spanning toward the soil surface. A helix situated at a higher level in the proximity of another helix can hinder the development of a passive wedge for the given helix, and the passive wedge is developed only for the upper helix. Therefore, the helix with the lower embedded depth (consequently with lower vertical stress) can be facilitated with the passive wedge, resulting in a decrease in the pullout bearing capacity. Following this, for a given space ratio, the bearing capacity and initial stiffness decrease with the number of helices, as the helices

As the depth of the buried helix increases, and with it the vertical effective stress, the load-bearing capacity increases.

5.3 Expanded Piles

Figs. 14(a) and 14(b) illustrate a comparison between the load-displacement curves of various pile types of expanded piles, (i.e., SE-extended, SE-non Extended, Bubble, and Wing piles) and some conventional and unconventional piles under compression and pullout loadings, respectively.

Detailed information regarding the mechanisms and specifications of the expanded piles can be found in Table 2 along with the associated references.

In terms of compression loading, the expanded piles generally demonstrate lower bearing capacity and initial stiffness when compared to conventional piles. Notably, Wing piles exhibit the best performance in terms of both bearing capacity and initial stiffness.

In the case of pullout loading, expanded piles demonstrate a significant advantage over other pile types. In simple terms, their bearing capacity increases by approximately 100%, especially for Bubble piles, and their initial stiffness surpasses that of other pile types. It's important to note that the slight exceedance in the initial stiffness of the box-shaped pile can be attributed to its larger cross-sectional area. It is evident that the highest pullout bearing capacities are observed for Bubble, SE-Expanded, and helical piles, primarily due to their deep failure mode.

The pullout bearing capacity of the expanded and helical piles surpasses that of conventional driven piles. The increased pullout bearing capacity can be attributed to the expanded segment's large diameter in the Bubble pile and the substantial embedment depth of the helix in the helical pile. However, the Wing pile, despite its superior performance under compression loading, exhibits a lower pullout capacity. This lower pullout capacity can be attributed to the cavity formed during the installation process over the expanded part of the pile.

5.4 General Comparisons

Fig. 15 illustrates a comparison in terms of the ultimate mobilized load of piles upon criteria of 10% diameter in two different relative densities under both compression and pullout loadings. As anticipated, pullout and compressive capacities have been increased by an increase in the relative density. The ratio of bearing capacity for driven piles in loose to medium-dense sand has been in the range of 2.5 – 4 under compressive loading. This ratio has been between 3 to 5 for pullout loading. Moreover, this ratio for piles with higher area, i.e., piles initiating larger displacements in soil, has been decreasing in a way that the least and most differences have been for closed-end piles and H-piles, respectively. The induced difference for helical piles has been lower compared to driven piles through variation in relative density. The ratio of ultimate load for medium-dense sand compared to loose sand has been between 2.5 – 3.3 and 2.5 – 4.3 for compressive and pullout loading conditions, respectively. I worth mentioning that in these piles, the ratio has been decreased by increasing the number and diameter of helices which can be due to an increase in disturbance of adjacent soil. This issue is because of more soil disturbance and strength reduction in medium-dense soil compared to loose sand.

The ratio of compressive to pullout capacity for helical and expanded piles has been higher compared to conventional piles. This ratio has been in the range of 5 - 6 and 3 - 4 for loose and medium-dense sands, respectively. Moreover, by comparing piles installed by driving and jacking, the ratio of compressive and pullout capacity has been higher for jacking-driven piles, ranging between 5 and 5.5. As expected, this ratio has been highly lower for helical piles, in a way that a range of 1.1 to 1.7 for loose sands and a range of 1.1 to 2.1 for medium-dense sands have been observed. The existing soil is disturbed during the installation of helical piles and this change in density is more excessive for medium-dense sand compared to loose sand, and therefore the difference between pullout and compressive capacity is higher for sand with medium density. Since the topsoil disturbance increases by an increase in the number and diameter of helices and realizing the role of topsoil in pullout capacity, by increasing the number and diameter of helices, the ratio of compressive capacity to pullout capacity rises.

6- Field Testing Research Sites

Numerous field tests were carried out at the Anzali and Babolsar sites to assess the behavior of various types of piles subjected to compression and pullout loads, as described in section 3.2. Fig. 16 provides a visual representation of the pile installation process, complete with a torque meter to record installation torque at different depths. Figs. 16(b) and 16(c) depict the setups for applying compressive and pullout loads.

The tested piles encompass a range of types, including conventional open-end piles, helical piles with 1 and 2 helices, and special piles. These piles were installed in sand deposits, and the investigation covered a multitude of geometric and practical characteristics. Notable factors studied included embedment depth, helix diameter, helix spacing to diameter ratio, and the impact of the installation method. The above-mentioned load test records are reviewed, addressed, and compiled. More details on pile characteristics, deposits, and loading types have been outlined in Table 4.

Fig. 17(a) and 17(b) depict the load-displacement curves for piles installed at the research sites, specifically Babolsar and Anzali, under both compression and pullout loadings, respectively. As for compression loading, illustrated in Fig. 17(a), four piles were installed at the Anzali site, encompassing a one-helix pile with rounded and square shaft shapes, a drilled displacement pile (featuring a small helix at the pile tip, as schematically depicted in Table 4), and a rounded driven pile.

Analyzing the load-displacement curves of piles installed at the Anzali site, it can deduced that the helical piles exhibit higher bearing capacities compared to the drilled and driven piles, attributed to their lower initial stiffness resulting from reduced soil disturbance during installation. It is crucial to note that the initial stiffness is primarily influenced by shaft resistance during the initial loading stages, significantly impacted by soil disturbance induced during installation.

Furthermore, a slight increase in bearing capacity is observed as the shaft shape transitions from square to round, owing to reduced soil disturbance in the rounded shaft.

Additionally, two helical piles were examined at the Babolsar site, specifically helical piles with two and three helices. The results reveal an increase in bearing capacity under compression loading corresponding to the number of helices. In Fig. 17(b), the load-displacement responses of piles installed at the Anzali site under pullout loading are illustrated. A substantial enhancement in pullout bearing capacity is observed among helical piles (both round and square shafts) compared to drilled or driven piles, underscoring the pronounced influence of helices in mobilizing pullout bearing capacity in contrast to compression loading. Similar to the compression loading, the helical pile with a round shaft demonstrates higher bearing capacity under pullout loading, attributed to reduced soil disturbance compared to the square shaft.

7. Scale-up of Model Piles to Prototype

In this investigation, diverse pile types were scrutinized and compared using the FCV device, complemented by field tests at two distinct research sites. To assess the applicability of the scaling-up method for FCV results concerning helical piles under both compression and pullout loadings, two sets of FCV tests were conducted under different conditions: (a) maintaining exact stress condition similarity, following the description by Sedran (2000), and (b) introducing a discrepancy in stress conditions.

The scaling-up of the results of physical modeling even under well-defined methods to simulate the prototype conditions might end up with discrepant results, as a simplified model under fully a controlled condition may fail to consider the all details perfectly. Therefore, it should be acknowledged the error exceedance between the results of the model and the prototype, particularly when the stress similarity is not satisfied.

The planned field tests at the Anzali and Babolsar research sites involved helical piles with one and two helices, respectively. Anticipated maximum vertical stresses in the vicinity of pile tips at both research sites are expected to be approximately 63 kPa. Supplementary FCV experiments were additionally performed on soils from Babolsar and Anzali, aiming to induce vertical stresses of 63, 80, and 100 kPa at the tip elevation of piles following the two specified methods. In-situ mass densities at both sites were determined using the Sand-Cone Method (i.e., ASTM D1556), resulting in average values of 19.5 kN/m^3 and 18.7 kN/m^3 for the Anzali and Babolsar sites, respectively. All attempts were made to ensure similarity in relative density between field and FCV experiments, confirmed through in-situ sampling subsequent to pressurizing the FCV chamber.

As outlined in Table. 1, the scaling-up factors for stress (i.e., λ_σ) for the settings suggested by Sedran (2000) and this study are respectively 1 and an arbitrary value. The selected λ_L for the supplementary FCV tests on the Anzali and Babolsar sands are 4.4 [-] and 4.67 [-], respectively. λ_σ values for the FCV tests with 63, 80, and 155 kPa are respectively 1, 0.79, and 0.41 [-]. It should be noted that λ_σ=1 [-] represents method (a) by which the stress similarity is maintained, whereas λ_σ ≈0.79 [-] and 0.41 [-] signify discrepancies in stress conditions between FCV and field tests.

Fig. 18 presents a comparison between the load-displacement curves of scaled-up FCV load-displacement curves (using the 10% of pile diameter criterion) for helical piles with one and two helices under different stress conditions (i.e., 63, 80, and 155 kPa) in contrast to corresponding field tests. It is evident that the scaled-up curves of FCV tests for both sites under 63 kPa, where stress similarity is maintained, closely align with the field curves (with an 11% exceedance in expected bearing capacity). In contrast, the predicted bearing capacity increases with induced vertical stresses, deviating from the field tests, especially under 155 kPa, where the stress discrepancy significantly exceeds real stresses, leading to a notable shift in the deformation regime.

However, concerning the scaled-up curves under 80 kPa, despite a stress discrepancy between the stress conditions, the difference between the field and predicted curves is less pronounced, providing a reasonable prediction of load-displacement curves.

8. Conclusions

This study is dedicated to evaluating the load-displacement behavior of various piles, examining both model-scale and full-scale scenarios. The investigation also delves into the impact of installation effects in the FCV-AUT physical modeling apparatus and extends to full-scale assessments conducted along the coastal line of the Caspian Sea. To accomplish this, over 40 model-scale and 10 full-scale records have been compiled. The studied piles fall into three main categories: conventional piles (jacking, driving, and drilled), helical piles, and expanded piles. Additionally, two different methods to scale up the load-displacement curves of FCV results were examined, considering the stress similarity (suggested by Sedran (2001) and discrepancy (i.e., examined in this study).

Among the various pile installation methods, those implemented through the jacking method demonstrated the highest ultimate load. This can be attributed to the lower soil disturbance around the pile and an increase in the relative density of the soil during the installation process. The ratio of compressive ultimate load for jacking piles, compared to H-shaped, open-end, and closed-end driven piles based on the 0.1D criteria, was 2.5, 2.1, and 1.7, respectively. For the pullout condition, these ratios were 1.4, 1.3, and 1.7 for the mentioned piles. Conversely, the precast-in-place pile exhibited the lowest ultimate load among the various methods. This is due to stress release in the soil around the pile after excavation, followed by the debris flow effect in the toe area. These factors result in soil disturbance and diminish the pile-soil interaction, leading to a reduced capacity.

Helical piles with S/D=3 demonstrated greater resistance compared to piles with S/D=1.5, attributed to a singular failure mode. In compressive loading, the lower helix played a crucial role, while under pullout loads, the upper helix ranked highest in resistance. The three-helix pile with S/D=3 exhibited the highest bearing capacity under compressive loading. Conversely, during pullout testing, the two-helix pile exhibited the greatest capacity, attributed to the substantial embedment depth of the upper helix. Additionally, the ratio of pullout to compressive capacity was highest for the one-helix pile compared to the others.

Two scale-up methods were investigated to anticipate the field load-displacement curves of helical piles, considering stress similarity and discrepancy. The results revealed that the scale-up method with stress similarity yielded accurate predictions, whereas stress discrepancy led to a notable deviation from field tests, especially in cases of significant discrepancies. Indeed, the stress similarity can relatively ensure that the soil behaves correspondingly. However, the scale-up method can be used in the case of stress discrepancy as long as no intense change in the soil's load-deformation regime occurs.

References

Al-Suhaily, Ahmed S, Ahmed S Abood, and Mohammed Y Fattah. 2018. Bearing capacity of uplift piles with end gates. Paper presented at the Proceedings of China-Europe Conference on Geotechnical Engineering: Volume 2.

Arabameri, Mohammad, and Abolfazl Eslami. 2021. "Microstructure and strength effect on bearing capacity of helical piles installed in golestan loess." *International Journal of Civil Engineering* 19:923-940.

Baca, Michal, and Wlodzimierz Brzakala. 2017. "Numerical modeling of pile installation influence on surrounding soil." *International Multidisciplinary Scientific GeoConference: SGEM* 17 (1.2):619-626.

Bak, Hamid Mortazavi, Amir M Halabian, Hamid Hashemolhosseini, and Mohammadali Rowshanzamir. 2021. "Axial response and material efficiency of tapered helical piles." *Journal of Rock Mechanics and Geotechnical Engineering* 13 (1):176-187.

Basu, Prasenjit, Monica Prezzi, and Dipanjan Basu. 2010. "Drilled displacement piles–current practice and design." *DFI Journal-The Journal of the Deep Foundations Institute* 4 (1):3-20.

Basu, Prasenjit, Monica Prezzi, and Rodrigo Salgado. 2014. "Modeling of installation and quantification of shaft resistance of drilled-displacement piles in sand." *International Journal of Geomechanics* 14 (2):214-229.

Byrne, BW, and GT Houlsby. 2015. "Helical piles: an innovative foundation design option for offshore wind turbines." *Philosophical Transactions of the Royal Society A: Mathematical, Physical and Engineering Sciences* 373 (2035):20140081.

Ebrahimipour, Amirhossein, and Abolfazl Eslami. 2024. "Analytical study of piles behavior for marine challenging substructures." *Ocean Engineering* 292:116514.

Eslami, Abolfazl, Donya Afshar, Hassan Moghadasi, and Davood Akbarimehr. 2023. "Numerical and Experimental Investigations of Interference Effect of Adjacent Buildings on Sand and Fill Deposits." *International Journal of Civil Engineering*:1-16.

Eslami, Abolfazl, Davood Akbarimehr, Esmail Aflaki, and Mohammad Mahdi Hajitaheriha. 2020. "Geotechnical site characterization of the Lake Urmia super-soft sediments using laboratory and CPTu records." *Marine Georesources & Geotechnology* 38 (10):1223-1234.

Esmailzade, Mohammad, Abolfazl Eslami, Ali Nabizadeh, and Esmail Aflaki. 2022. "Effect of cone diameter on determination of penetration resistance using a FCV." *International Journal of Civil Engineering*:1-14.

Fakharian, Kazem, Morteza Shafiei, and Salar Hafezan. 2022. "Investigation of soil setup effects on pile response in clay considering over-consolidation ratio and installation method through physical modeling." *Canadian Geotechnical Journal* (ja).

Fateh, Amir Mansour Askari, Abolfazl Eslami, and Ahmad Fahimifar. 2018. "A study of the axial load behaviour of helical piles in sand by frustum confining vessel." *International Journal of Physical Modelling in Geotechnics* 18 (4):175-190.

Fattah, Mohammed Y, Raid R Al-Omari, and Shaimaa H Fadhil. 2020. "Load sharing and behavior of single pile embedded in unsaturated swelling soil." *European Journal of Environmental and Civil Engineering* 24 (12):1967-1992.

Fattah, Mohammed Y, and Wissam HS Al-Soudani. 2016. "Bearing capacity of closed and open ended pipe piles installed in loose sand with emphasis on soil plug."

Fattah, Mohammed Y, Bushra S Zbar, and Faris S Mustafa. 2017. "Vertical vibration capacity of a single pile in dry sand." *Marine Georesources & Geotechnology* 35 (8):1111-1120.

Fellenius, Bengt H. 2004. "Unified design of piled foundations with emphasis on settlement analysis." In *Current practices and future trends in deep foundations*, 253-275.

Garnier, Jacques, Christophe Gaudin, Sarah M Springman, PJ Culligan, D Goodings, D Konig, B Kutter, R Phillips, MF Randolph, and Luc Thorel. 2007. "Catalogue of scaling laws and similitude questions in geotechnical centrifuge modelling." *International Journal of Physical Modelling in Geotechnics* 7 (3):01-23.

Gavin, Kenneth, Paul Doherty, and Ali Tolooiyan. 2014. "Field investigation of the axial resistance of helical piles in dense sand." *Canadian Geotechnical Journal* 51 (11):1343-1354.

Hajitaheriha, Mohammad Mahdi, Davood Akbarimehr, Amin Hasani Motlagh, and Hossein Damerchilou. 2021. "Bearing capacity improvement of shallow foundations using a trench filled with granular materials and reinforced with geogrids." *Arabian Journal of Geosciences* 14:1-14.

Heins, Evelyn, Britta Bienen, Mark F Randolph, and Juergen Grabe. 2020. "Effect of installation method on static and dynamic load test response for piles in sand." *International Journal of Physical Modelling in Geotechnics* 20 (1):1-23.

Horvath, Robert G, and Dieter Stolle. 1996. "Frustum confining vessel for testing model piles." *Canadian Geotechnical Journal* 33 (3):499-504.

Jardine, RJ, BT Zhu, P Foray, and ZX Yang. 2013. "Measurement of stresses around closed-ended displacement piles in sand." *Geotechnique* 63 (1):1-17.

Karimi, AH, A Eslami, M Zarrabi, and J Khazaei. 2017. "Study of pile behavior by improvement of confining soils using frustum confining vessel." *Scientia Iranica* 24 (4):1874-1882.

Kaviani-Hamedani, Farzad, Mohammad Esmailzade, Kianoush Adineh, Morteza Shafiei, and Danial Shirkavand. 2024. "Quantifying three-dimensional sphericity indices of irregular fine particles from 2D images through sequential sieving tests." *Granular Matter* 26 (1):13.

Khazaei, Javad, and Abolfazl Eslami. 2016. "Geotechnical behavior of helical piles via physical modeling by Frustum Confining Vessel (FCV)." *International Journal of Geography and Geology* 5 (9):167-181.

———. 2017. "Postgrouted helical piles behavior through physical modeling by FCV." *Marine Georesources & Geotechnology* 35 (4):528-537.

Kumar, PR. 2007. "Scaling laws and experimental modelling of contaminant transport mechanism through soils in a geotechnical centrifuge." *Geotechnical and Geological Engineering* 25:581-590.

Kurian, Nainan P, and Syed J Shah. 2009. "Studies on the behaviour of screw piles by the finite element method." *Canadian Geotechnical Journal* 46 (6):627-638.

Lanyi-Bennett, Stephen A, and Lijun Deng. 2019. "Axial load testing of helical pile groups in glaciolacustrine clay." *Canadian Geotechnical Journal* 56 (2):187-197.

Liu, Cong, Xiaowei Tang, Huanwei Wei, Pengpeng Wang, and Honghua Zhao. 2020. "Model tests of jacked-pile penetration into sand using transparent soil and incremental particle image velocimetry." *KSCE Journal of Civil Engineering* 24 (4):1128-1145.

Livneh, Ben, and M Hesham El Naggar. 2008. "Axial testing and numerical modeling of square shaft helical piles under compressive and tensile loading." *Canadian Geotechnical Journal* 45 (8):1142-1155.

Lutenegger, Alan J, and Cristina de HC Tsuha. 2015. Evaluating installation disturbance from helical piles and anchors using compression and tension tests. Paper presented at the Proceedings of the 15th Pan-American Conference on Soil Mechanics and Geotechnical Engineering, Buenos Aires, Argentina.

Mansour, Mohamed A, and M Hesham El Naggar. 2022. "Optimization of grouting method and axial performance of pressure-grouted helical piles." *Canadian Geotechnical Journal* 59 (5):702-714.

Nabizadeh, Farhad, and Asskar Janalizadeh Choobbasti. 2017. "Field study of capacity helical piles in sand and silty clay." *Transportation Infrastructure Geotechnology* 4:3-17.

Paik, Kyuho, and Rodrigo Salgado. 2004. "Effect of pile installation method on pipe pile behavior in sands." *Geotechnical Testing Journal* 27 (1).

Perlow, Jr, Michael. 2011. "Helical pile acceptance criteria, design guidelines, and load test verification." In *Geo-Frontiers 2011: Advances in Geotechnical Engineering*, 94-102.

Sedran, Gabriel. 1999. "Experimental and analytical study of a frustum confining vessel."

Shirani, Seyed Sajad, Abolfazl Eslami, Amirhossein Ebrahimipour, and Moses Karakouzian. 2023. "Dominant factors in MiniCone, CPT and pile correlations: A data-based approach." *Deep Underground Science and Engineering* 2 (4):346-358.

Shojaei, Ebrahim, Abolfazl Eslami, and Navid Ganjian. 2021. "Self-expanded piles: A new approach to unconventional piles development." *Marine Georesources & Geotechnology* 39 (1):115-128.

Spagnoli, G. 2013. "Some considerations regarding the use of helical piles as foundation for offshore structures." *Soil mechanics and foundation engineering* 50 (3):102-110.

Spagnoli, G, and K Gavin. 2015. Helical piles as a novel foundation system for offshore piled facilities. Paper presented at the Abu Dhabi International Petroleum Exhibition and Conference.

Spagnoli, G, K Gavin, C Brangan, and S Bauer. 2015. "In situ and laboratory tests in dense sand investigating the helix-to-shaft ratio of helical piles as a novel offshore foundation system." *Frontiers in Offshore Geotechnics* 3:643-648.

Tang, Chong, and Kok-Kwang Phoon. 2016. "Model uncertainty of cylindrical shear method for calculating the uplift capacity of helical anchors in clay." *Engineering Geology* 207:14-23.

Tsuha, Cristina de Hollanda Cavalcanti, Thiago da Costa Santos, Gérard Rault, Luc Thorel, and Jacques Garnier. 2013. "Influence of multiple helix configuration on the uplift capacity of helical anchors." *Congrès International de Mécanique des Sols et de Géotechnique* 18.

Zarrabi, Mohammad, and Abolfazl Eslami. 2016. "Behavior of piles under different installation effects by physical modeling." *International Journal of Geomechanics* 16 (5):04016014.

Table 1 Scaling factors for FCV apparatus

Parameters	Scaling Factor	Setting of factors†	Suggested Scaling Factor
Displacement and dimensions	λ_L	λ_L	λ_L
Area	λ_A	λ_L^2	λ_L^2
Volume	λ_V	λ_L^3	λ_L^3
Mass	λ_M	λ_L^3	λ_L^3
Density	λ_ρ	1	1
Stress	λ_σ	1	λ_σ
Strain	λ_ε	1	1
Force	λ_F	λ_L^2	$\lambda_\sigma \lambda_L^2$
Modulus	λ_E	1	λ_σ

†: suggested by Sedran et al. (2001)

Table 2 Index properties of Anzali and Babolsar sands

Parameter	**Anzali sand**	**Babolsar sand**
G_s	2.69	2.78
$e_{\max}$	0.89	0.876
$e_{\min}$	0.69	0.637
$\gamma_{d,\max}(kN/m^3)$	16.9	17.0
$\gamma_{d,\min}(kN/m^3)$	15.8	14.82
$D_{50}(mm)$	0.21	0.18
C_u	2.1	1.22
C_c	1.1	1.67

Table 3 Various model piles installed and tested in FCV-AUT

No.	Ref.	Foundation Type and Category	Pile Specification	Tested Material	Soil relative density (%)	Installation & Testing
01	Zarrabi and Eslami 2016)	(I) Conventional Pile Closed-End Pile 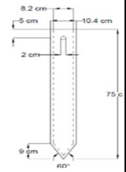	Outer diameter= 90 Inner diameter = 80 L/D = 7 D_f = 750	Babolsar Sand	45-50	Driven, Compression & Tension
02	Zarrabi and Eslami 2016)	(I) Conventional Pile H-Shape Pile 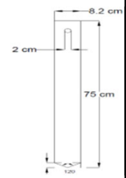	A * B = 80 * 80 L/D = 8 D_f = 750	Babolsar Sand	45-50	Jacking, Compression & Tension
03	Zarrabi and Eslami 2016	(I) Conventional Pile Open-End Pile 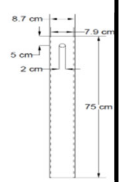	Outer diameter= 90 Inner diameter = 80 L/D = 9 D_f = 750	Babolsar Sand	45-50	Driven, Compression & Tension
04	Zarrabi and Eslami 2016	(I) Conventional Pile 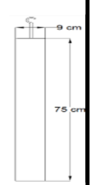	Outer diameter= 90 L/D = 8 D_f = 750	Babolsar Sand	45-50	Drilled, Compression & Tension
05	Zarrabi and Eslami 2016	(I) Conventional Pile 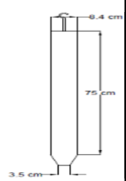	Outer diameter=90 L/D = 9 D_f = 750	Babolsar Sand	45-50	Driven, Compression & Tension
06	Zarrabi and Eslami 2016	(I) Conventional Pile 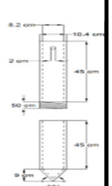	Outer diameter= 90 Inner diameter = 82 L/D = 7 D_f = 750	Babolsar Sand	45-50	Jacking, Compression & Tension
07	Zarrabi and Eslami 2016	(I) Conventional Pile 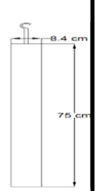	Outer diameter= 90 L/D = 9 D_f = 750	Babolsar Sand	45-50	precast-in-place, Compression & Tension

08	Zarrabi and Eslami 2016	(I) Conventional Pile 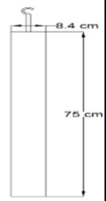	A * B = 80 * 80 L/D = 8 D_f = 750	Babolsar Sand	45-50	Driven, Compression & Tension
12	Beigi & Eslami, 2018	(II) Helical Pile 1 Helix 	d_{shaft}=32 d_{helix}=90 D_f= 750	Anzali sand	20-25 45-50	Torque, Compression & Tension
13	Beigi & Eslami, 2018	(II) Helical Pile 2 Helices 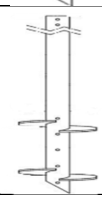	d_{shaft}=32 d_{helix}=90 S/D = 1.5 D_f= 750	Anzali sand	20-25 45-50	Torque, Compression & Tension
14	Beigi & Eslami, 2018	(II) Helical Pile 2 Helices 	d_{shaft}=32 d_{helix}=90 S/D = 3 D_f= 750	Anzali sand	20-25 45-50	Torque, Compression & Tension
15	Beigi & Eslami, 2018	(II) Helical Pile 3 Helices 	d_{shaft}=32 d_{helix}=90 S/D = 1.5 D_f= 750	Anzali sand	20-25 45-50	Torque, Compression & Tension
16	Beigi & Eslami, 2018	(II) Helical Pile 3 Helices 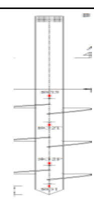	d_{shaft}=32 d_{helix}=90 S/D = 3 D_f= 750	Anzali sand	20-25 45-50	Torque, Compression & Tension
17	Fateh, Eslami, and Fahimifar 2018	(II) Helical Pile 1 Helix 	d_{shaft} = 34 d_{helix} = 70 D_f = 750	Anzali Sand	20-25 45-50	Torque, Compression & Tension
18	Fateh, Eslami, and Fahimifar 2018	(II) Helical Pile 2 Helices 	d_{shaft} = 32 d_{helix} = 70 S/D = 3 D_f = 750	Anzali Sand	20-25 45-50	Torque, Compression & Tension

19	Fateh, Eslami, and Fahimifar 2018	(II) Helical Pile 3 Helices 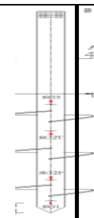	d_{shaft} = 32 d_{helix} = 70 S/D = 1.5 D_f = 750	Anzali Sand	20-25 45-50	Torque, Compression & Tension
20	Khazai & Eslami, 2016	(II) Helical Pile 2 Helices 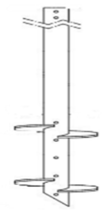	d_{shaft}=32 d_{helix}=64 D_f= 750	Babolsar Sand	45-50	Compression & Tension
21	Shojaei, Eslami, and Ganjian 2021	(II) Helical Pile 1 Helix 	d_{shaft}=32 d_{helix}=120 D_f= 750	Anzali Sand	45-50	Torque, Compression & Tension
22	Shojaei, Eslami, and Ganjian 202	(III) Special Pile Wing Pile 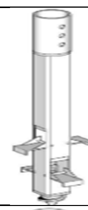	d =80 D_f= 750	Anzali Sand	45-50	Torque, Compression & Tension
23	Shojaei, Eslami, and Ganjian 2021	(III) Special Pile Self-Expanded Pile 	d =60 D_f= 750	Anzali Sand	45-50	Torque, Compression & Tension
24	Shojaei, Eslami, and Ganjian 2021	(III) Special Pile Bubble Pile 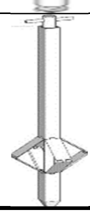	d =50 D_f= 750	Anzali Sand	45-50	Torque, Compression & Tension

Table 1 Various full-scale piles installed and tested along the Caspian Sea shoreline

No.	Reference	Foundation Type & Category	Pile Characteristics	Confined Soil	Installation & Testing
01	Shojae & Eslami, 2020	**(I) Conventional Pile** **Open-End Pile** 	$d = 114$ $D_f = 3300$	Anzali Sand	Driven, Compression & Tension
02	Shojae & Eslami, 2020	**(II) Helical Pile** **Round shaft** **1 Helix** 	$d_{shaft}=114$ $d_{helix}=250$ $D_f= 3300$	Anzali Sand	Torque, Compression & Tension
03	Shojae & Eslami, 2020	**(II) Helical Pile** **Square shaft** **1 Helix** 	$d_{shaft}=114$ $d_{helix}=250$ $D_f= 3300$	Anzali Sand	Torque, Compression & Tension
04	Shojae & Eslami, 2020	**(III) Special Pile** **Drilled Displacement Pile** 	$d =114$ $D_f= 3300$	Anzali Sand	Torque, Compression& Tension
05	Ahmadnexhad & Eslami, 2023	**(II) Helical Pile** **2 Helices** 	$d_{shaft}=114$ $d_{helix}=250$ $S/D = 1.5$ $D_f= 3500$	Babolsar Sand	Torque, Compression
06	Ahmadnexhad & Eslami, 2023	**(II) Helical Pile** **2 Helices** 	$d_{shaft}=11.4$ $d_{helix}=250$ $S/D = 3$ $D_f= 3500$	Babolsar Sand	Torque, Compression

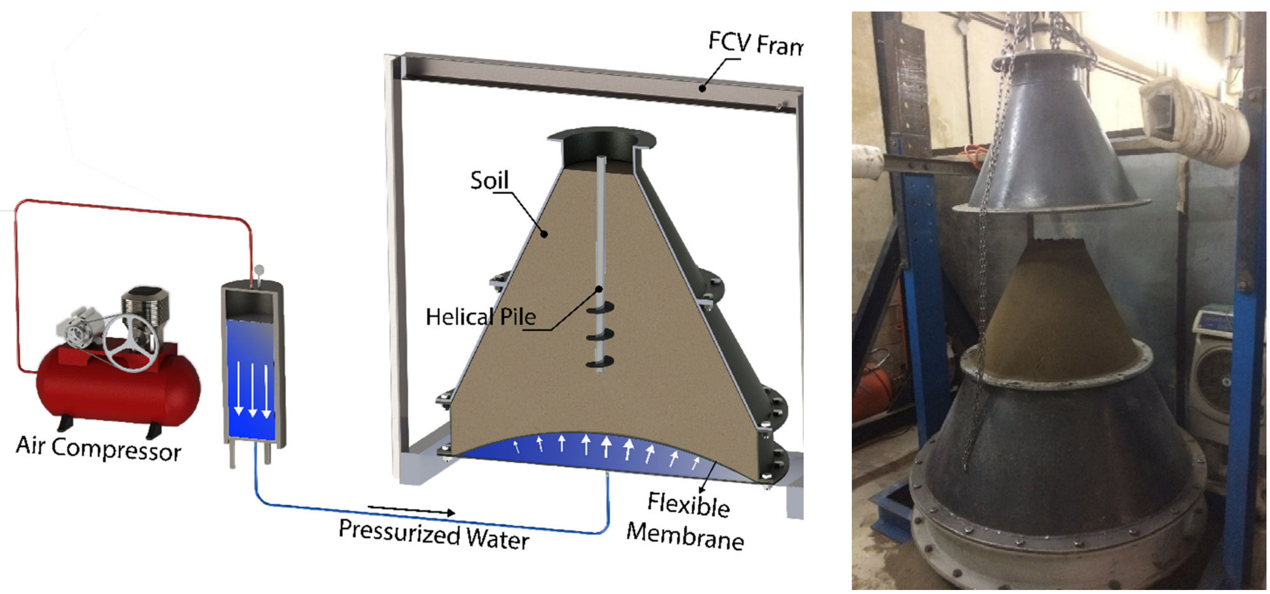

(a)

(b)

Fig 1. FCV-AUT: a) Schematic; b) Photograph

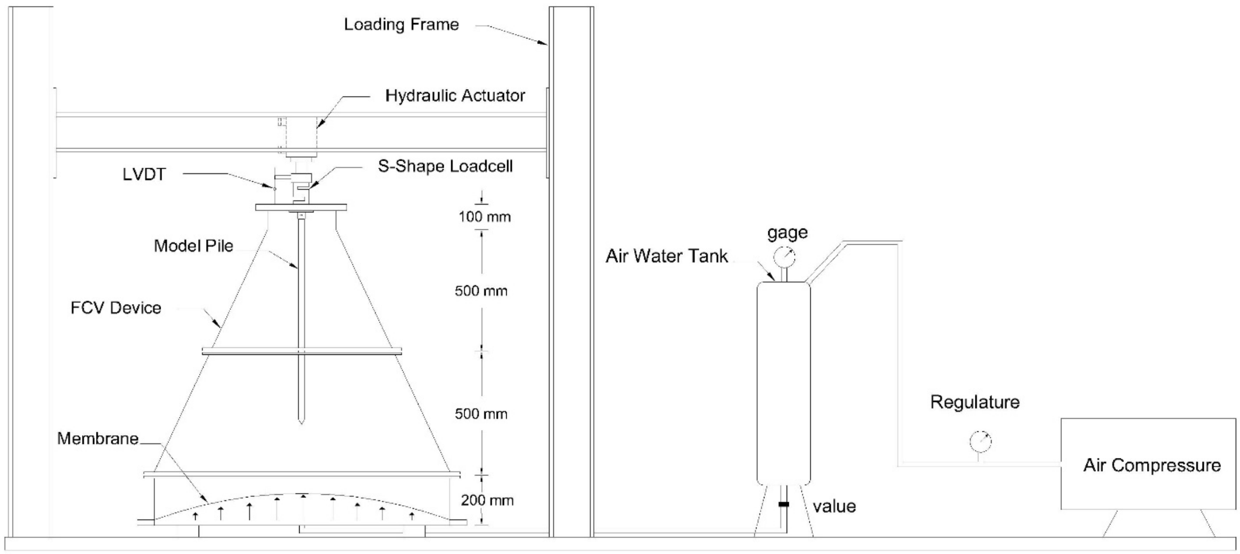

Fig. 2 A diagram of the Frustum Confining vessel and detail of the bottom pressure system

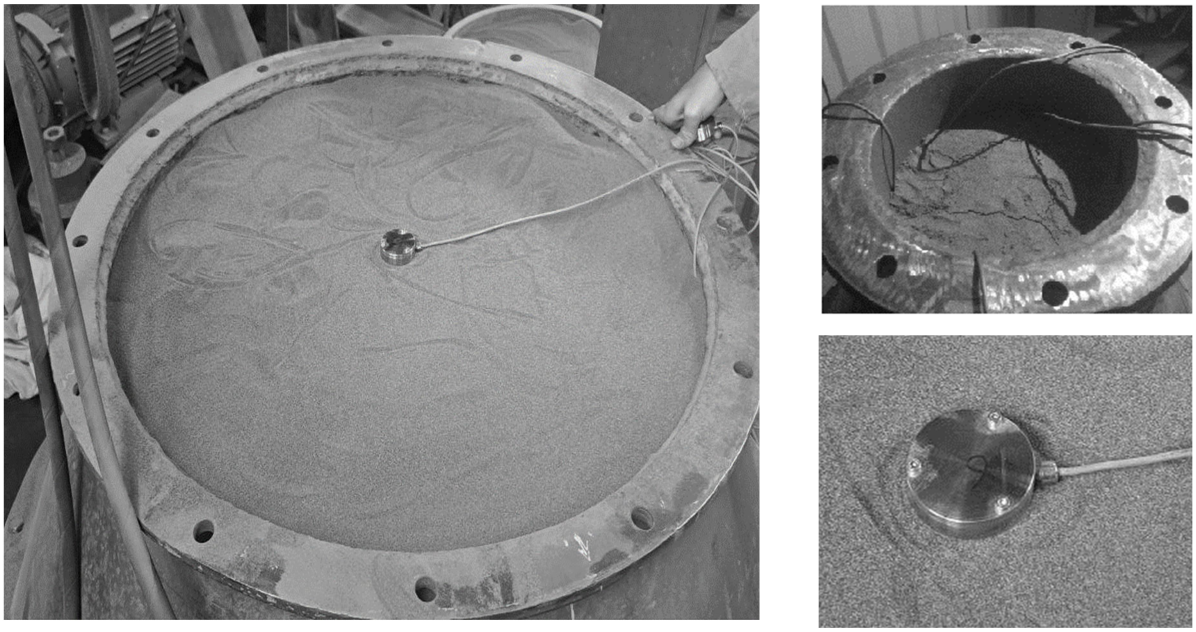

Fig. 3 Soil pressure cell installation in FCV to measure vertical and lateral stress

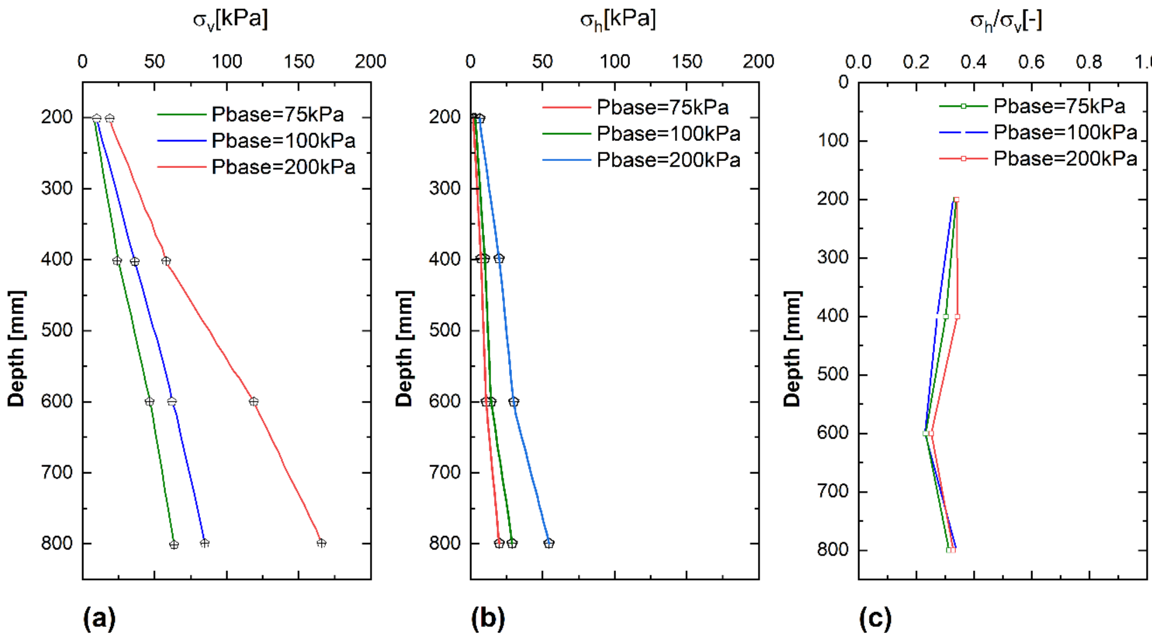

Fig. 4 Vertical, horizontal stress distribution, and the ratio of horizontal to vertical stress in depth for different applied pressures to the base of AUT-FCV

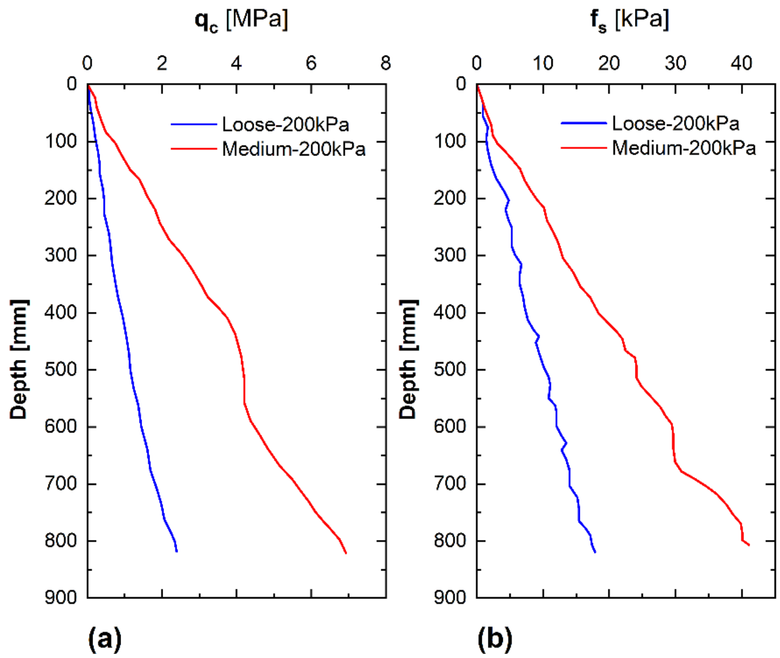

Fig. 5 CPT measurements in two different sand layers having different initial relative densities under a base pressure of 200kPa: (a) Cone resistance; (b) Sleeve friction

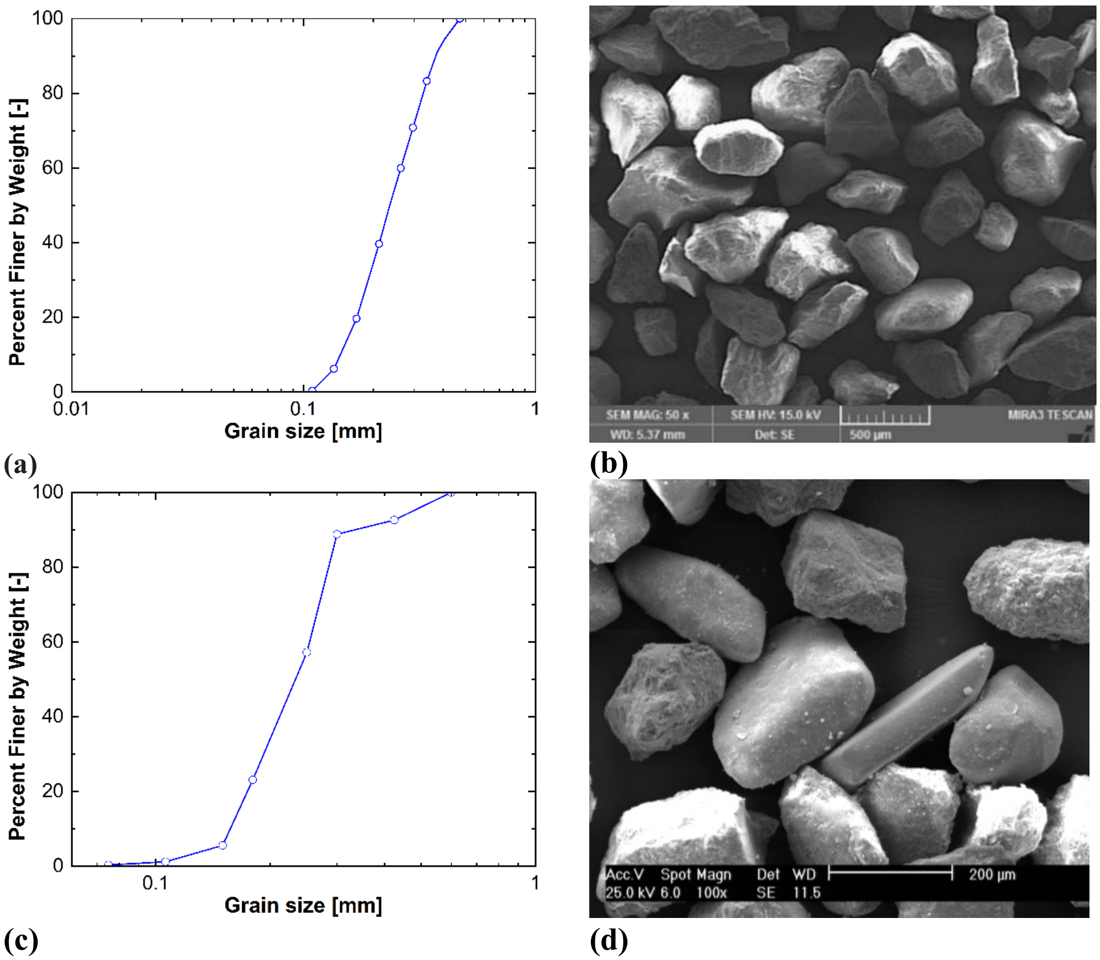

Fig. 6 Tested materials: (a) and (b) Anzali sand grading curve and grain-scale SEM; (c) and (d) Babolsar sand grading curve and grain-scale SEM

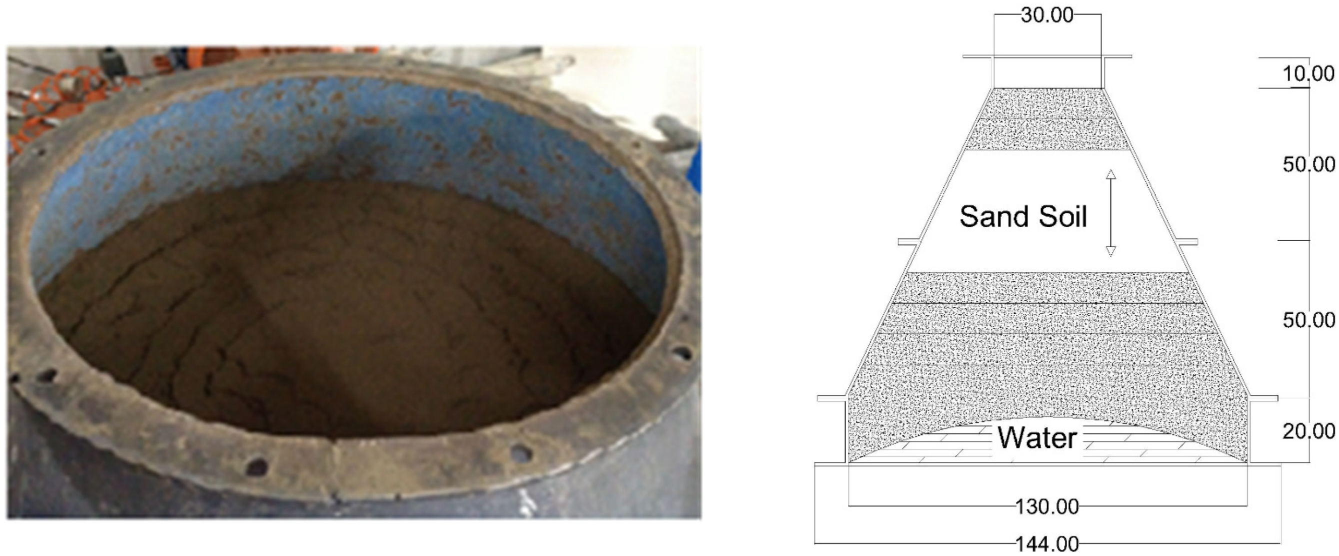

(a)

(b)

Fig. 7 Soil preparation procedure: (a) soil deposited inside the lower part of FCV-AUT; (b) schematic cross-section of FCV-AUT

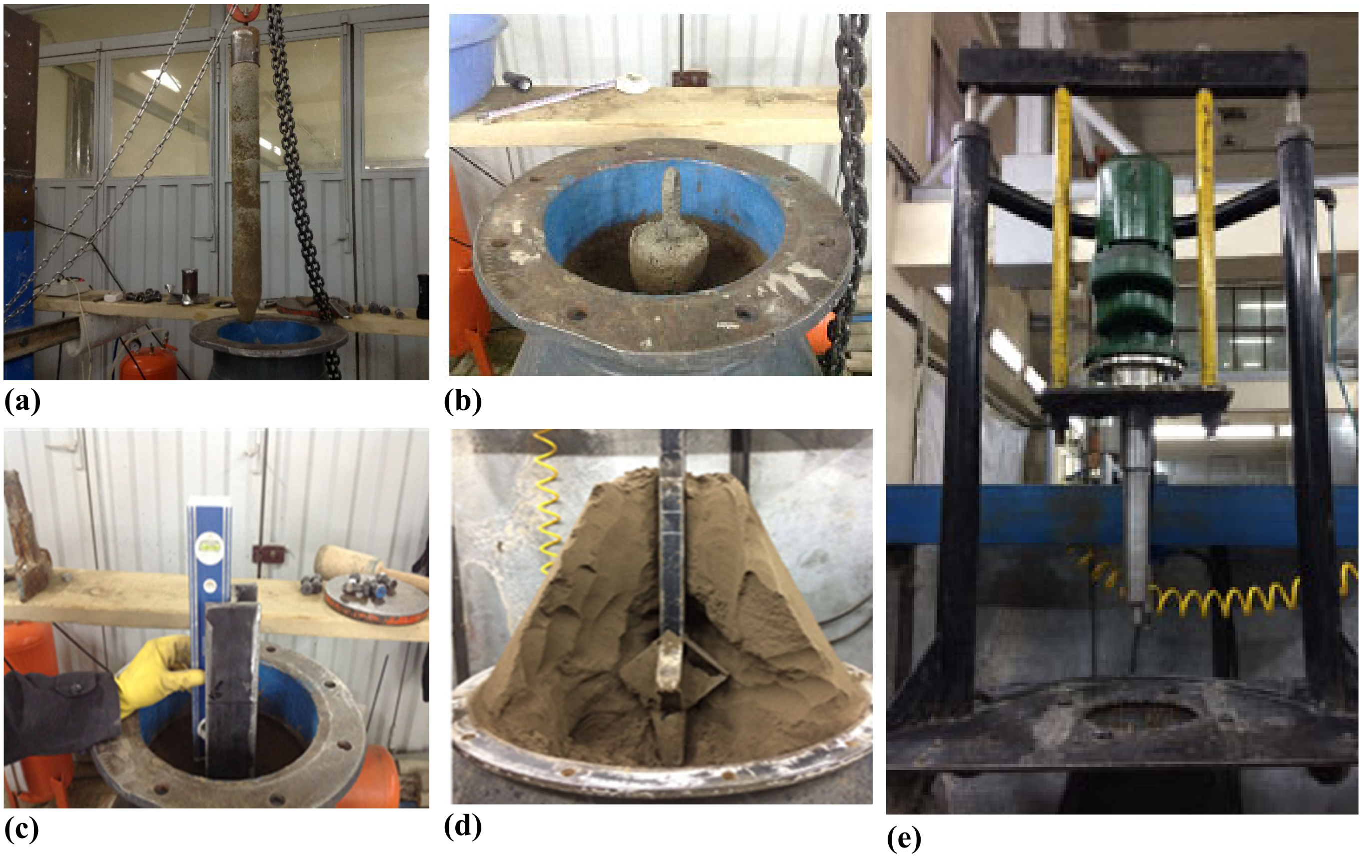

Fig. 8 Installation of pile models in the FCV-AUT: (a) precast-in-place pile; (b) drilled shaft (c) driven ; (d) expanded; (e) Torque motor and meter device

(a) (b)

Fig. 9 Arrangement of a typical pile during the loading stage: (a) Pullout test; (b) Compression test

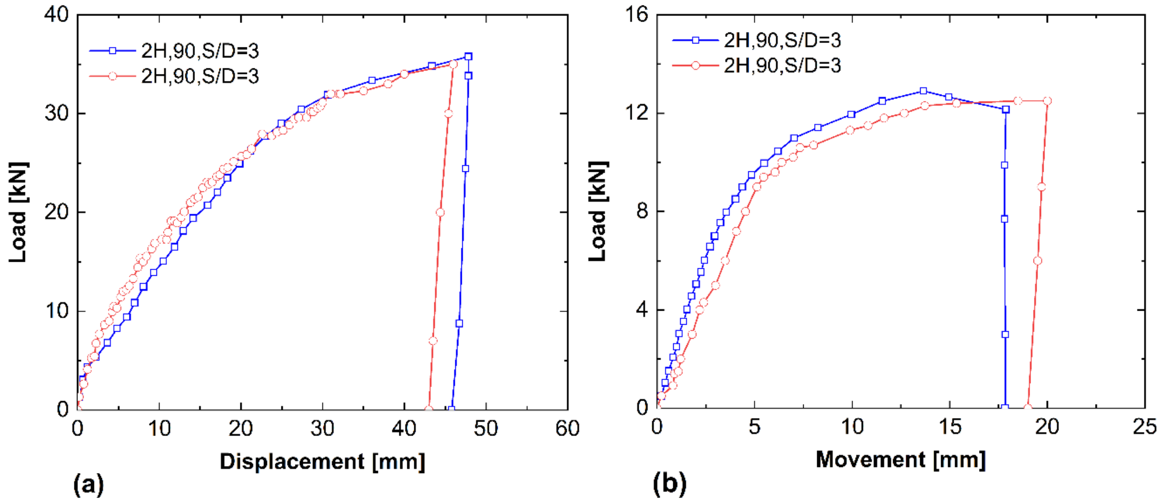

Fig. 10 Repeatability Load-displacement diagram of for 2 helix helical piles with S/D=3 a) Compression b) Pullout

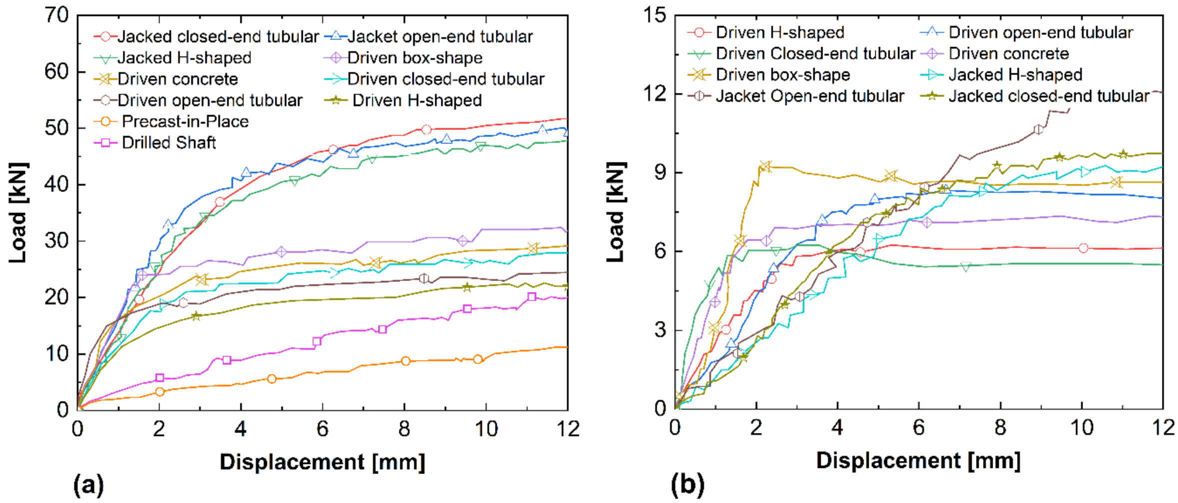

Fig. 11 Load-displacement diagram of jacking and driven piles a) Compression b) Pullout

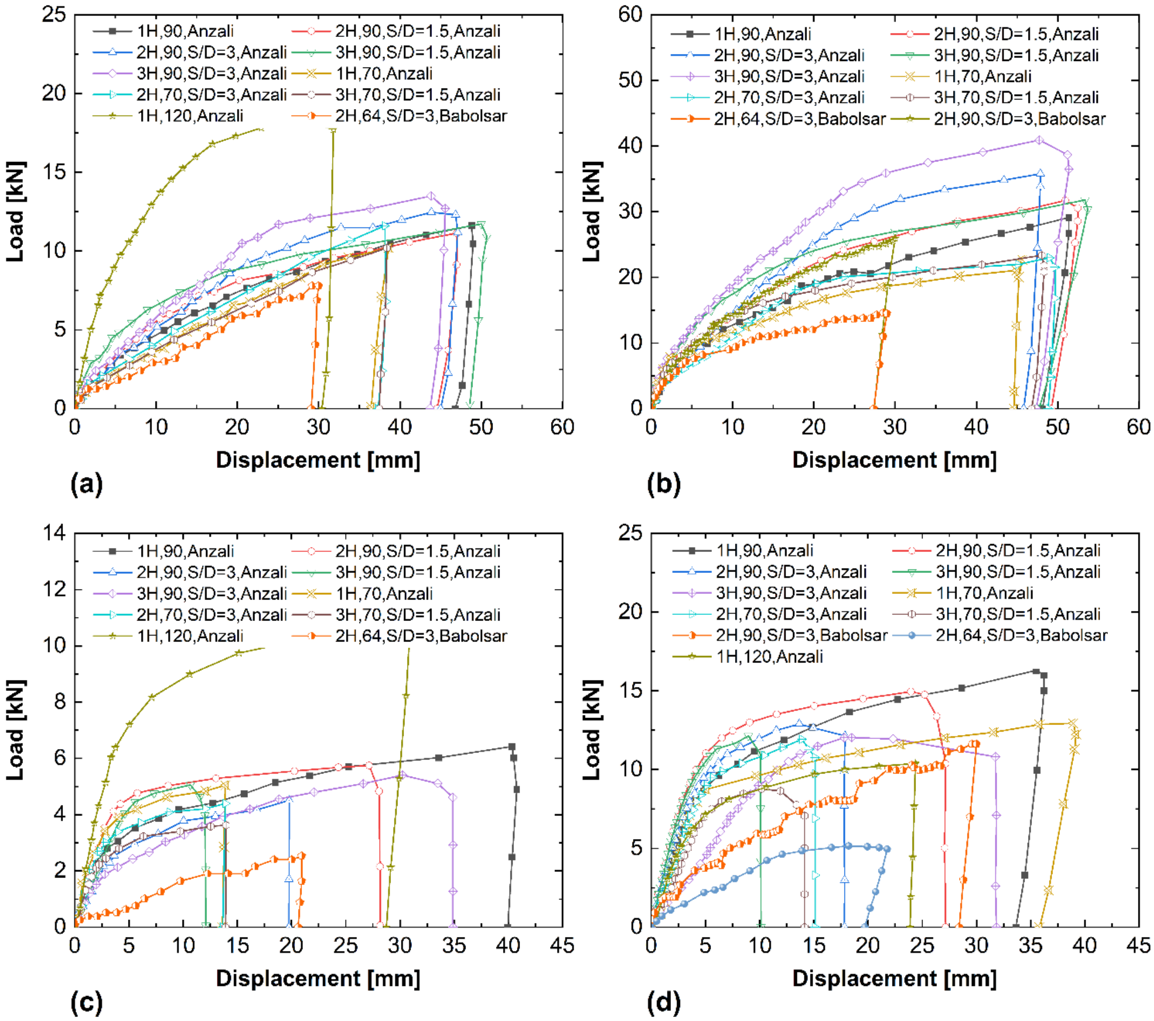

Fig. 12 Helical piles load-displacement diagrams: a) Compression, loose; b) Compression, medium; c) Pullout, loose d) Pullout, medium

723 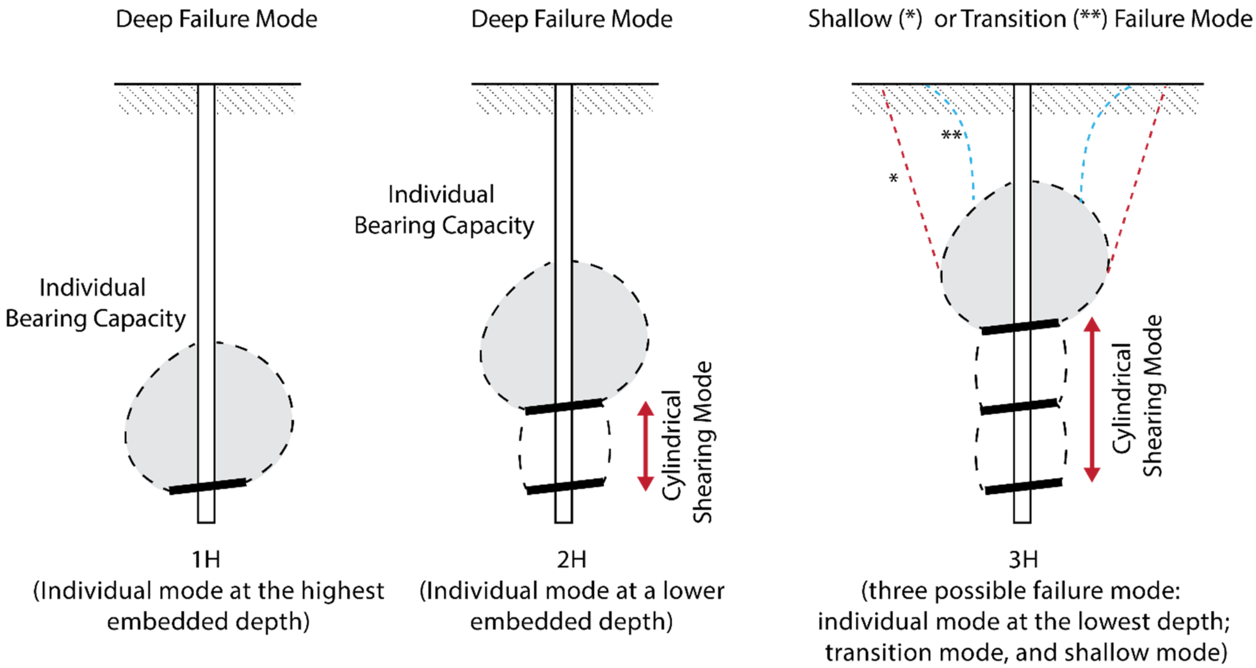

724 **Fig. 13** Different failure modes in helical piles

725

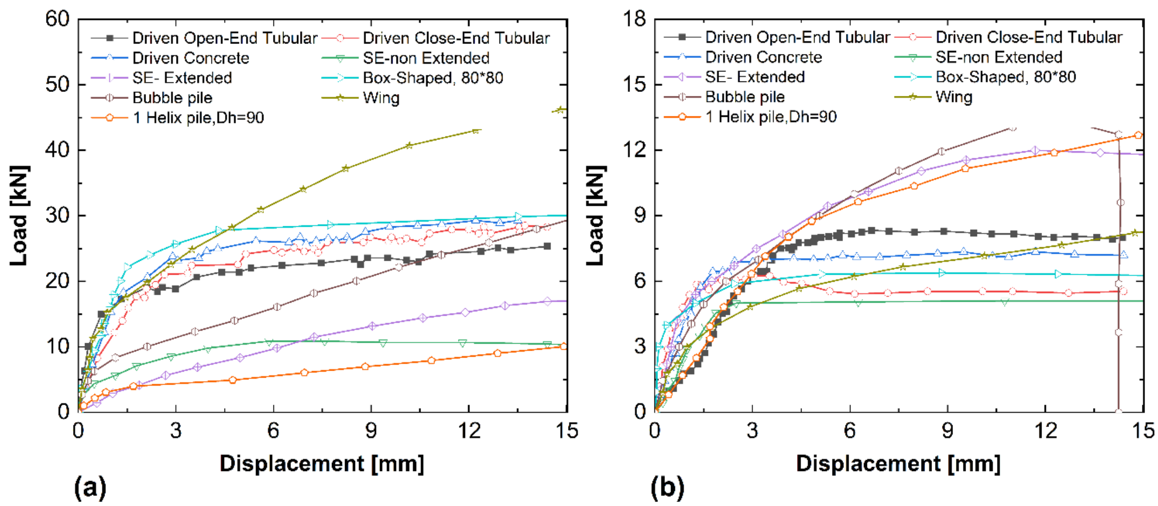

Fig. 14 Load-displacement diagrams of expanded piles under: (a) compression loading; (b) pullout loading

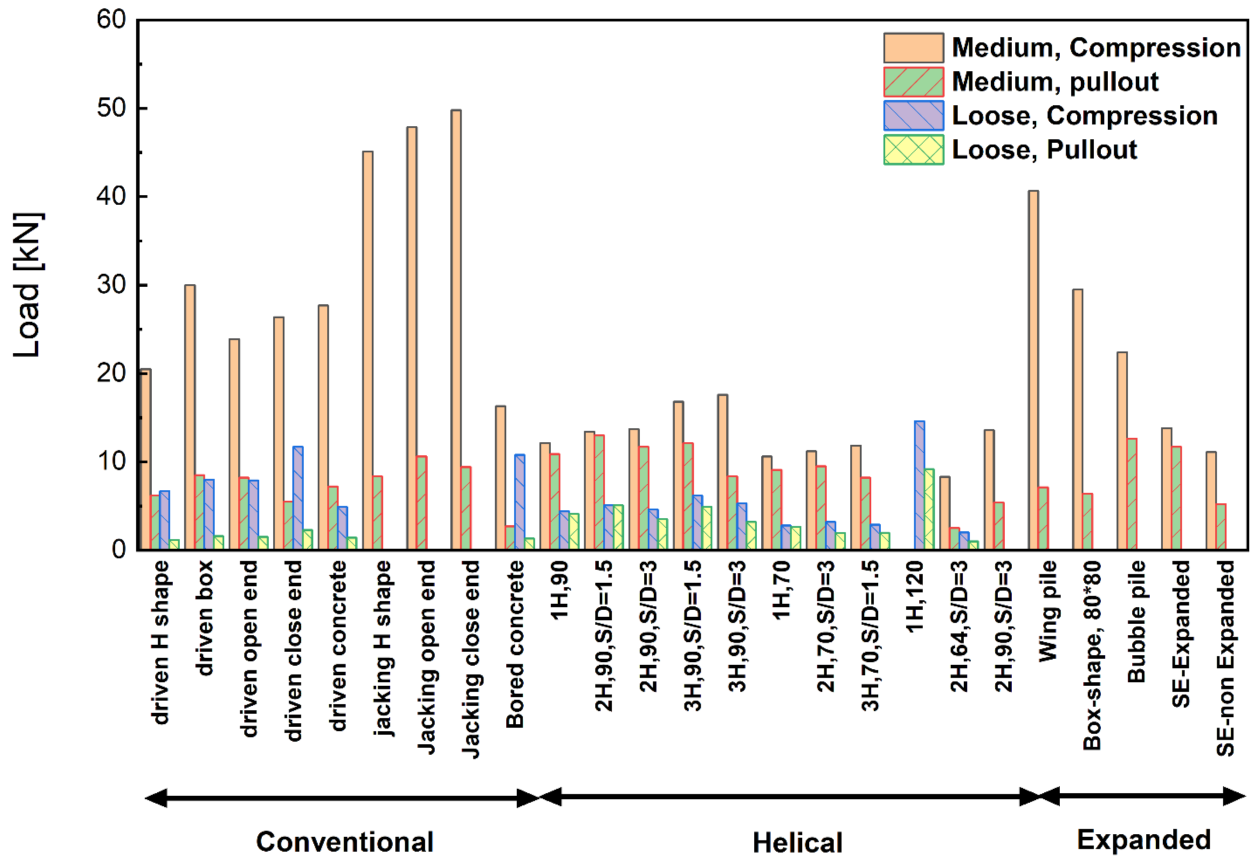

Fig. 15 A comparison of bearing capacity based on 10% of pile diameter criteria for different pile types under compression and pullout loadings

(a) (b) (c)

Fig. 16 Site testing: (a) Installation procedure; (b) Compression testing setup; (c) Pullout testing setup

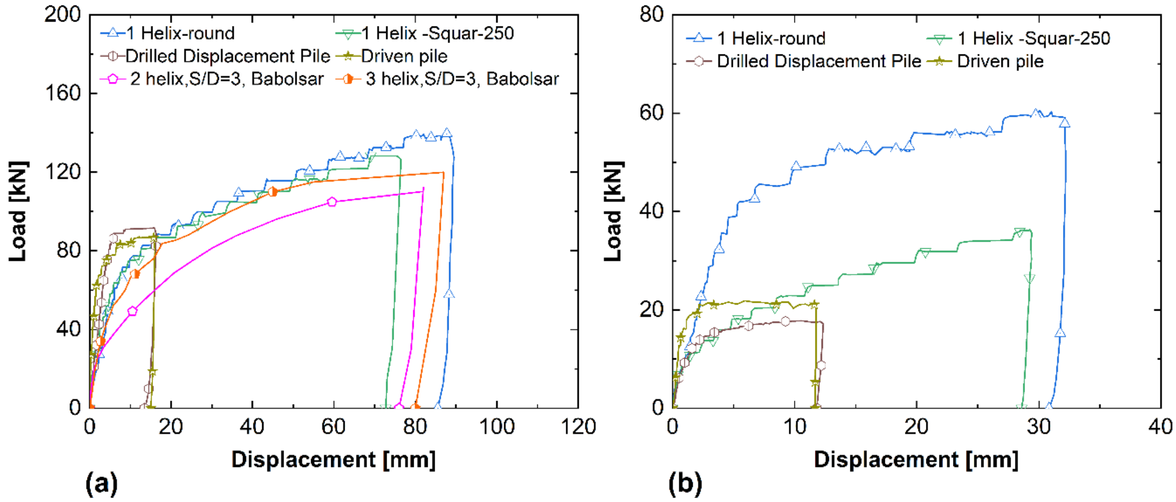

Fig. 17 Load-displacement curves of different full-scale piles in Anzali and Babolsar sites under: (a) compression loading; (b) pullout loading

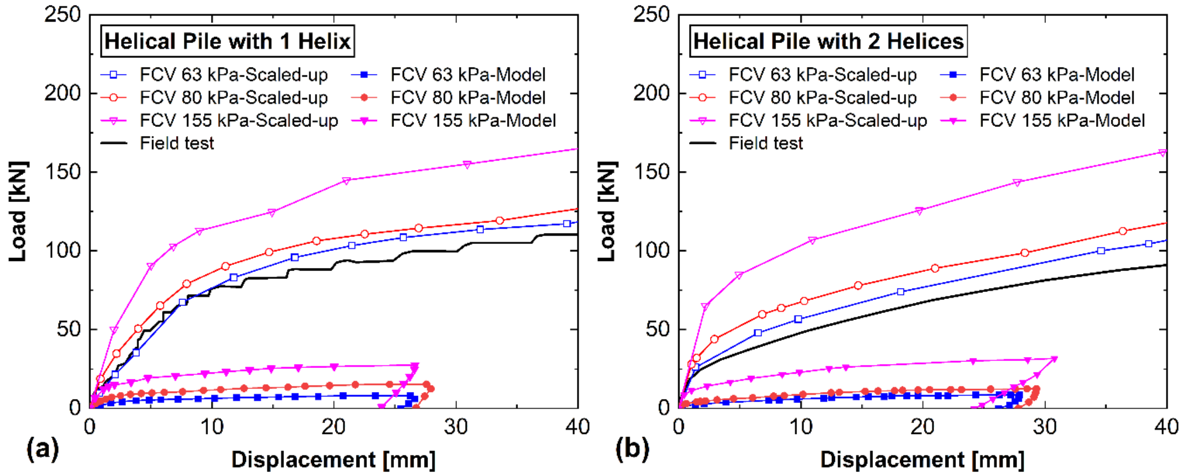

Fig. 18 Comparison of load-displacement curves for the model, field test, and predicted prototype piles for Helical Piles with: (a) 1 Helix at the Anzali site; (b) 2 Helices at the Babolsar Site